Article | Received 18 October 2024; Revised 28 July 2025; Accepted 14 August 2025; Published 21 August 2025
https://doi.org/10.55092/mt20250004

Switching control of maglev yaw system based on average dwell time via backstepping approach

Xiuli Wang[1,2], Qingyang Chen[1] and Jianye Gong[3,*]

[1] College of Information Engineering, Zhejiang University of Technology, Hangzhou 310023, Zhejiang Province, China
[2] Zhejiang Hengjiu Transmission Technology Inc., Ltd., Zhuji 311800, Zhejiang Province, China
[3] College of Information Engineering, Yangzhou University, Yangzhou 225127, Jiangsu Province, China

* Correspondence author; E-mail: jygong@yzu.edu.cn.

Highlights:

- A novel maglev yaw system is introduced to serve as a replacement for conventional gear-driven yaw mechanisms in wind turbines.
- Backstepping controllers are designed for both dynamic suspension subsystem and yawing suspension subsystem to ensure global stability and trajectory convergence.
- An average dwell time switching strategy is developed to guarantee exponential stability of the entire MYS.

Abstract: The stability control of a maglev yaw system (MYS) in wind turbines is investigated by replacing the conventional gear-driven yaw mechanism with magnetic levitation technology. The MYS comprises two subsystems: the Dynamic Suspension Subsystem (DSS) and the Yawing Suspension Subsystem (YSS), between which the system switches during operation. To prevent mechanical damage, it is essential to ensure the stability of both the individual subsystems and the overall switched system. Firstly, physical and mathematical models of DSS and YSS are developed, followed by the design of backstepping controllers to stabilize each subsystem. Then, a switching strategy based on the average dwell time method is proposed to guarantee the stability of the entire system. Finally, simulation results validate the effectiveness of the proposed control scheme in maintaining the stability of both subsystems and the overall MYS.

Keywords: maglev yaw system; dynamic suspension subsystem; yawing suspension subsystem; backstepping approach; average dwell time

1. Introduction

The yaw system is a critical component of horizontal-axis wind turbines, playing a vital role in wind energy utilization and the overall performance of the turbine. Such systems are associated with several limitations, including structural complexity, periodic lubrication requirements, reliance on multiple motors, maintenance difficulties, and a relatively high fault rate. Thus, it is particularly important and urgent to design a novel yaw system for rotating accurately to the wind with high stability and easy maintenance.

For this reason, yawing control of a MYS is achieved adopting maglev-driving technique instead of the traditional gear-driving technique in [1]. The maglev yawing process consists of three subprocesses: levitation, suspension and rotation at the equilibrium position, and landing aligned with the wind direction. Among them, the levitation and landing phases are referred to as Dynamic Suspension (DS), while the suspension and rotation at the equilibrium position are termed Yawing Suspension (YS). That means MYS includes two subsystems: the DSS and YSS. When the wind direction changes, MYS works with switching between DSS and YSS. However, for the conventional wind turbines and the maglev yaw systems, most researches focus on the control strategies of the systems without considering the switching problem [1–3]. In MYS systems with multiple operating modes (DSS and YSS), the absence of an effective switching strategy can lead to inefficiency, instability, and even mechanical failure when facing faults, disturbances, or load variations. To address this, a well-designed switching strategy is essential to enhance MYS's reliability, efficiency, and long-term stability, especially under varying conditions.

As for the switching algorithm, the multi-mode operation for switched systems is not a simple superposition of different modes, and the switching operation among different operating modes would be likely to result in infinite multiple switching in finite time [4,5]. The switching between different stable operation modes may lead to the instability of the whole switched system [6,7]. Designing dwell time approach is an efficient approach for the whole system's stability [8–10]. In [11], exponential stabilization for switched positive linear systems is guaranteed by multiple time-varying Lyapunov functions and dwell-time switching techniques. Compared to dwell time, Average Dwell Time (ADT) allows switching signals to satisfy average frequency constraints over a long-time span, providing greater flexibility to the switching rule. In [12], the ADT method is extended into Markov jump systems and a non-fragile sliding mode observer is designed to effectively handle time-varying delays and packet loss issues, ensuring finite-time boundedness. A neural control method based on ADT is proposed in [13], ensuring system stability through mode-dependent ADT, preventing singularity, and optimizing the transient tracking error behavior. Mutation-free transmission control along with the ADT method is utilized to address the stability and robustness of time-delay switched systems, improving the smooth transition of the system.

The switching stability problem can be roughly divided into two classes: arbitrary switching stability and constrained switching stability [14–16]. The stability of systems under arbitrary switching sequences is mainly based on multi Lyapunov theory and linear matrix inequality (LMI) method [17,18]. There are also researches on constrained switching stability. In [19], the Lyapunov theory of logical dynamic systems with average dwell-time method, is put forward for ensuring the point stability of the considered switched logical dynamic systems. In [20], stability conditions are derived using multiple Lyapunov functions and mode-dependent average dwell-time, which relaxes the conservation caused by common Lyapunov function and average dwell-time.

Extending the above discussed average dwell time method to magnetic levitation systems, this study aims to ensure stable switching between the DSS and the YSS in the MYS via ADT method. To maintain stability under varying conditions, controllers of subsystems are designed using the backstepping approach. Additionally, an ADT-based switching rule is developed to enable smooth transitions between subsystems. Compared to fixed dwell-time strategies, ADT intelligently regulates switching frequency through stability-oriented time constraints, minimizing excessive transitions and mechanical shocks.

The remainder of this paper is organized as follows. Section 2 presents the physical models of the DSS and YSS, which are subsequently formulated using appropriate state-space representations. In Section 3, the models are simplified via homeomorphic transformations, and the design procedures for stable controllers based on the backstepping method are proposed for both DSS and YSS. Then, an average dwell time approach is adopted to design the switching rule of the switched system. Section 4 contains the simulation results of the proposed method. Finally, concluding remarks are addressed in Section 5.

2. The MYS and modeling of DSS and YSS

Figure 1 illustrates the structure of the MYS, which mainly comprises a magnetic levitation and drive system, a support system, and guide bearings. The magnetic levitation and drive system includes a synchronous disc motor (consisting of suspension electromagnets and a stator), air-gap sensors, and a controller.

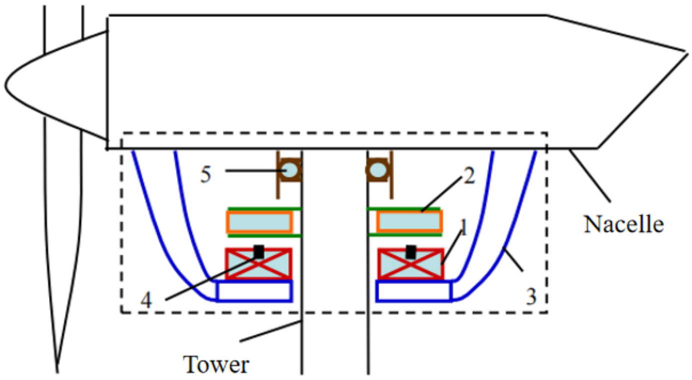

Figure 1. Structural sketch of MYS. 1: suspension electromagnet (rotor); 2: stator; 3: magnetic suspension support system; 4: air gap sensor; 5: guide bearing.

Subsection 2.1 presents the physical models of DSS and YSS, which are subsequently transformed into mathematical models via a suitable state-space representation in Subsection 2.2.

2.1. The physical models of DSS and YSS

The MYS is an electromechanical platform developed in our laboratory as an alternative to traditional gear-driven yaw mechanisms, as illustrated in Figure 2. It is activated in response to changes in wind direction. The yawing process includes four stages: lift-off, static levitation, rotation at the equilibrium point, and landing at the upwind position. During the lift-off stage, the suspension electromagnets and the wind turbine nacelle rise together under the action of the levitation force until they reach the equilibrium position. During the landing stage, the suspension electromagnets and the nacelle descend together to the final position under the combined effects of gravity and the levitation force.

To achieve stable operation, the MYS is designed as a switched system comprising two subsystems: the DSS and the YSS. The MYS integrates a magnetic suspension and driving system with a supporting structure that includes the nacelle platform, tower, and suspension bracket. A synchronous disc motor drives the system, using a rotor formed by the suspension electromagnet and a stator.

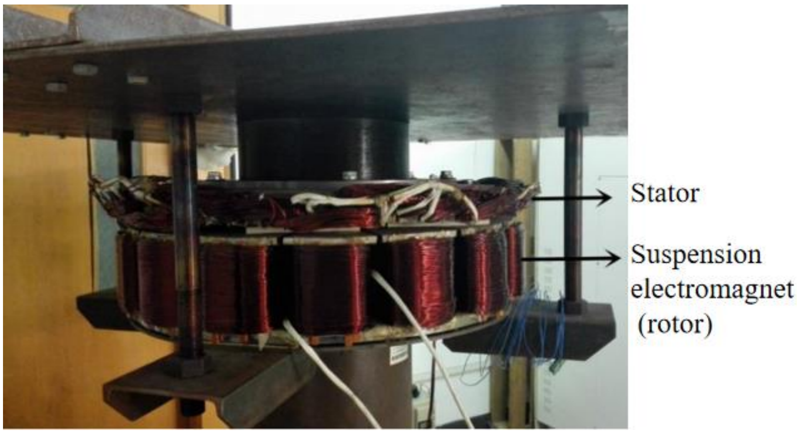

Figure 2. Prototype of the MYS.

2.1.1. Model of DSS

During the DS process, as illustrated in Figure 3, the suspended object either moves upward toward the equilibrium position (levitation) with acceleration $\ddot{\delta}$, or downward to the resting position (landing) with acceleration $\ddot{\delta}$. Accordingly, the physical model of the DSS is obtained as follows [1]:

$$\begin{cases} mg - F = m\ddot{\delta} \\ u_D(t) = Ri(t) + \dfrac{k}{\delta(t)} \cdot \dfrac{di(t)}{dt} - \dfrac{ki(t)}{\delta^2(t)} \cdot \dfrac{d\delta(t)}{dt} \\ F = \dfrac{1}{2}k \cdot \dfrac{i^2(t)}{\delta^2(t)}. \end{cases} \tag{1}$$

where m denotes the mass associated with the suspension object, F denotes the magnetic lift force, $u_D(t)$ represents the DC exciting voltage applied to the suspension electromagnet $u(t)$ during the DS process, R is the resistance that arises from the rotor's winding circuit, $i(t)$ stands for the DC exciting current, δ indicates the air gap for levitation, measured as the distance between the stator and the levitation electromagnet. $k = \mu_0 N^2 S/2$, in which μ_0 is permeability of vacuum, N is the number of coil turns, and S is the effective area of the magnetic poles of the suspension electromagnet.

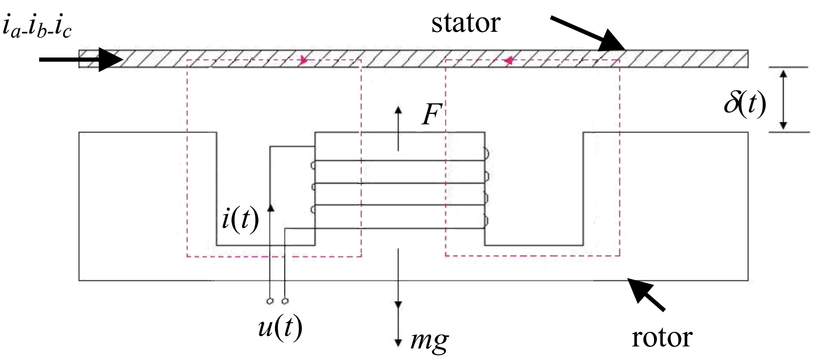

Figure 3. Mechanical model of MYS.

2.1.2. Model of YSS

As shown in Figure 3, during the YS process, the stator is energized by a three-phase AC current with a low frequency, thus the rotor will rotate at the equilibrium position with the nacelle up to the wind direction.

The flux linkage produced by the stator current in the dq reference frame can be written as:

$$\begin{bmatrix}\psi_d\\ \psi_q\end{bmatrix}=\begin{bmatrix}L_d i_d\\ L_q i_q\end{bmatrix}=\begin{bmatrix}L_d\left[\cos\theta\left(\frac{\sqrt{2}}{3}i_a-\frac{\sqrt{2}}{6}i_b-\frac{\sqrt{2}}{6}i_c\right)+\sin\theta\left(\frac{\sqrt{6}}{6}i_b-\frac{\sqrt{6}}{6}i_c\right)\right]\\ L_q\left[-\sin\theta\left(\frac{\sqrt{2}}{3}i_a-\frac{\sqrt{2}}{6}i_b-\frac{\sqrt{2}}{6}i_c\right)+\cos\theta\left(\frac{\sqrt{6}}{6}i_b-\frac{\sqrt{6}}{6}i_c\right)\right]\end{bmatrix},$$

where ψ_d, ψ_q are the flux linkages; L_d, L_q represent the d and q component of inductance respectively; i_d, i_q are the stator currents, $\theta=\omega t$ is the rotation angle, ω is angular velocity.

According to the field-orientation principle, ψ_d could make the MYS rotate, and ψ_q could change the magnetic energies stored in the air gap, which will influence the suspension control of MYS. The suspension control input $u_Y(t)$ can be described as

$$\begin{aligned}u_Y(t)&=Ri(t)+\frac{d\left(\psi(t)+\psi_q(t)\right)}{dt}\\&=Ri(t)+\frac{k}{\delta(t)}\cdot\frac{di(t)}{dt}-\frac{ki(t)}{\delta^2(t)}\cdot\frac{d\delta(t)}{dt}+\frac{d\psi_q(t)}{dt},\end{aligned}$$

where $u_Y(t)$ is the DC exciting voltage of the suspension electromagnet (rotor) $u(t)$ in the YS process, $\psi(t)$ represents the flux linkage generated by the rotor's DC excitating current $i(t)$.

Thus, the physical model of YSS can be given by rewriting equation (1):

$$\begin{cases}mg-F=m\ddot{\delta}\\ u_Y(t)=Ri(t)+\dfrac{d\left(\psi(t)+\psi_q(t)\right)}{dt}\\ F=\dfrac{1}{2}k\cdot\dfrac{i^2(t)}{\delta^2(t)}.\end{cases}\qquad(2)$$

2.2. Mathematical models of DSS and YSS

Subsection 2.1 has given the physical models of DSS and YSS, which are described by equations (1) and (2) respectively. The mathematical models of DSS and YSS should be established before designing the controller and switching rule.

The state variables x_1, x_2, x_3 of MYS are defined as:

$$\begin{bmatrix}x_1\\x_2\\x_3\end{bmatrix}=\begin{bmatrix}e\\ \dot{\delta}(t)\\ i(t)\end{bmatrix},$$

where $e=\delta(t)-\delta_{ref}(t)$ and denotes the trajectory error, in which $\delta_{ref}(t)$ is the reference trajectory.

From the integration of equations (1) and (2), the corresponding state-space expressions for DSS and YSS are constructed as follows:

$$\begin{bmatrix}\dot{x}_1\\ \dot{x}_2\\ \dot{x}_3\end{bmatrix}=\begin{bmatrix}x_2-\dot{\delta}_{ref}(t)\\ g-\dfrac{k}{2m}\cdot\dfrac{{x_3}^2}{(x_1+\delta_{ref}(t))^2}\\ -\dfrac{x_1+\delta_{ref}(t)}{k}Rx_3+\dfrac{x_3}{x_1+\delta_{ref}(t)}x_2\end{bmatrix}+\begin{bmatrix}0\\ 0\\ \dfrac{x_1+\delta_{ref}(t)}{k}\end{bmatrix}u(t)+\frac{x_1+\delta_{ref}(t)}{k}M, \tag{3}$$

where $u(t)=u_D(t)$ and $M=M_D=0$ in the process of DSS; and $u(t)=u_Y(t)$, $M=M_Y=\begin{bmatrix}0\\ 0\\ -\frac{d[L_q\cdot i_q(t)]}{dt}\end{bmatrix}$ in the process of YSS.

3. Controller and switching rule design

In this subsection, a coordinate transformation is used to simplify the mathematical model (3). Then, to ensure the stability of the two subsystems, the backstepping method is adopted to design the controllers of DSS and YSS. The switching rule is designed using the average dwell time method to maintain the stability of the switched system.

3.1. Model transformation

Due to system's nonlinear complexity, system (3) of the MYS is simplified by employing the coordinate transformation defined as follows:

$$\begin{aligned}z_1&=x_1\\ z_2&=x_2-\dot{\delta}_{ref}(t)\\ z_3&=g-\frac{k}{2m}\cdot\frac{{x_3}^2}{(x_1+\delta_{ref}(t))^2},\end{aligned} \tag{4}$$

From equation (4), the inverse transformation can be derived as

$$\begin{aligned}x_1&=z_1\\ x_2&=z_2+\dot{\delta}_{ref}(t)\\ x_3&=\sqrt{\frac{2m}{k}(z_1+\delta_{ref}(t))^2(g-z_3)},\end{aligned} \tag{5}$$

As transformations (4) and (5) are both continuous, transformation (4) represents a homeomorphic coordinate transformation.

Consequently, the reformulation of system (3) is given by:

$$\begin{aligned}\dot{z}_1 &= z_2 \\ \dot{z}_2 &= z_3 - \ddot{\delta}_{ref}(t) \\ \dot{z}_3 &= \frac{x_3}{m(z_1 + \delta_{ref}(t))}(Rx_3 - u(t) - M),\end{aligned} \tag{6}$$

3.2. Controller design and stability analysis of DSS and YSS

3.2.1. Controller design

The stable operation of MYS is based on the stability of each subsystem and the switched rule. According to equation (6), controller $u(t)$ is designed by backstepping approach to ensure the stability of each subsystem. As the recursive process of backstepping is stopped once the control input $u(t)$ is obtained, the design process can be divided into three steps.

Step1: In z_1-subsystem, new variables $\xi_1 = z_1$, $\xi_2 = z_2 - \alpha_1(\xi_1)$ are defined, where $\alpha_1(\xi_1)$ is applied as a virtual control. For subsystem:

$$\dot{\xi}_1 = \xi_2 + \alpha_1(\xi_1),$$

a Lyapunov function is introduced as:

$$V_1 = \frac{1}{2}{\xi_1}^2.$$

Its derivative is:

$$\dot{V}_1 = \xi_1(\xi_2 + \alpha_1(\xi_1)). \tag{7}$$

If the virtual control law is picked as $\alpha_1(\xi_1) = -k_1\xi_1$, where $k_1 > 0$, $\alpha_1(\xi_1)$ is a smooth function and $\alpha_1(0) = 0$, then equation (7) could be rendered into:

$$\dot{V}_1 = -k_1{\xi_1}^2 + \xi_1\xi_2. \tag{8}$$

Step 2: For $\{\xi_1, \xi_2\}$-subsystem, according to $\xi_2 = z_2 - \alpha_1(\xi_1)$, the following equations can be obtained:

$$\dot{\xi}_2 = \dot{z}_2 - \dot{\alpha}_1(\xi_1) = z_3 - \ddot{\delta}_{ref}(t) - \dot{\alpha}_1.$$

where α_1 is a virtual control variable, and its derivative is given by:

$$\dot{\alpha}_1 = -k_1\dot{\xi}_1 = -k_1\xi_2 + k_1^2\xi_1$$

Thus, the overall expression becomes:

$$\dot{\xi}_2 = k_1\xi_2 - {k_1}^2\xi_1 + z_3 - \ddot{\delta}_{ref}(t). \tag{9}$$

Then, a new state variable is defined as $\xi_3 = z_3 - \alpha_2(\xi_1, \xi_2)$, where $\alpha_2(\xi_1, \xi_2)$ is regarded as a virtual input. The Lyapunov function is augmented as

$$V_2 = \frac{1}{2}{\xi_1}^2 + \frac{1}{2}{\xi_2}^2$$

Its derivative function is:

$$\begin{aligned}\dot{V}_2 = -k_1{\xi_1}^2 + \xi_2(\xi_1 + k_{\ 1}\xi_2 - k_1^2\xi_1 + \xi_3 \\ + \alpha_2(\xi_1, \xi_2) - \ddot{\delta}_{ref}(t))\end{aligned} \tag{10}$$

One chooses:

$$\alpha_2(\xi_1, \xi_2) = k_1^2\xi_1 - \xi_1 - k_{\ 1}\xi_2 - k_2\xi_2 + \ddot{\delta}_{ref}(t)$$

where $k_2 > 0$, and $\alpha_2(\xi_1, \xi_2)$ is a smooth function. Then it is substituted into equation (10), there is:

$$\dot{V}_2 = -k_1{\xi_1}^2 - k_{\ 2}{\xi_2}^2 + \xi_2\xi_3$$

Step3: For $\{\xi_1, \xi_2, \xi_3\}$-system, ξ_3 satisfies the following equation:

$$\begin{aligned}\dot{\xi}_3 = \frac{x_3}{m(z_1 + \delta_{ref}(t))}(Rx_3 - u(t) - M) + (1 + k_1k_2)z_2 \\ +(k_1 + k_2)z_3 - (k_1 + k_2)\ddot{\delta}_{ref}(t) - \dddot{\delta}_{ref}(t)\end{aligned} \tag{11}$$

In this system, the Lyapunov function is constructed as:

$$V_3 = \frac{1}{2}{\xi_1}^2 + \frac{1}{2}{\xi_2}^2 + \frac{1}{2}{\xi_3}^2 \tag{12}$$

Its derivative function is:

$$\begin{aligned}\dot{V}_3 &= -k_1{\xi_1}^2 - k_{\ 2}{\xi_2}^2 + \xi_3\ \ (\xi_2 + \dot{\xi}_3) \\ &= -k_1{\xi_1}^2 - k_{\ 2}{\xi_2}^2 + \xi_3[\frac{R{x_3}^2}{m(z_1 + \delta_{ref}(t))} \\ &\quad - \frac{x_3}{m(z_1 + \delta_{ref}(t))}u(t) - \frac{x_3}{m(z_1 + \delta_{ref}(t))}M \\ &\quad + (1 + k_1k_2)z_2 + (k_1 + k_2)z_3 - (k_1 + k_2)\ddot{\delta}_{ref}(t) \\ &\quad - \dddot{\delta}_{ref}(t) + \xi_2]\end{aligned} \tag{13}$$

If the control input $u(t)$ is selected as:

$$\begin{aligned}u(t) = \frac{m(z_1 + \delta_{ref}(t))}{x_3}[(k_1 + k_3 + k_1k_2k_3)z_1 \\ +(k_1k_2 + k_1k_3 + k_2k_3 + 2)z_2 + (k_1 + k_2 + k_3)z_3 \\ -(k_1 + k_2 + k_3)\ddot{\delta}_{ref}(t) - \dddot{\delta}_{ref}(t) + \frac{R{x_3}^2}{m(z_1 + \delta_{ref}(t))}] - M\end{aligned} \tag{14}$$

where $k_3 > 0$, the derivative function (13) could be rewritten as:

$$\dot{V}_3 = -k_1{\xi_1}^2 - k_{\ 2}{\xi_2}^2 - k_3{\xi_3}^2 \leq 0 \tag{15}$$

3.2.2. Stability analysis

For the whole switched system, its working process needs to ensure the stable operation of the two subsystems, otherwise, the abnormal operation of MYS may occur, and even the mechanical structure would be damaged. Therefore, it is necessary to analyze the stability property for the two subsystems.

Theorem 1: For the system (3), assume that the control law is established as equation (14).

(I) During the DSS and YSS processes, the air gap length $\delta(t)$, its velocity $\dot{\delta}(t)$ and the exciting current $i(t)$ maintain globally bounded.

(II) When $t\to\infty$, $\delta(t)$ asymptotically converges globally to its reference trajectory $\delta_{ref}(t)$, while the velocity $\dot{\delta}(t)$ asymptotically converges globally to its reference velocity $\dot{\delta}_{ref}(t)$ in the DSS and YSS.

Proof: The proof procedure is given as follows:

(I) As the coordinate transformation (6) is a homeomorphic transformation, and the original system (3) is equivalent to the new system (6). To prove that the gap length $\delta(t)$, the velocity $\dot{\delta}(t)$ and the exciting current $i(t)$ are globally bounded, we just need to prove that z_1, z_2 and z_3 in equation (6) are globally bounded, respectively.

For the $\{\xi_1, \xi_2, \xi_3\}$-system, the Lyapunov function is selected as:

$$V_3 = \frac{1}{2}{\xi_1}^2 + \frac{1}{2}{\xi_2}^2 + \frac{1}{2}{\xi_3}^2$$

According to equation (13), the derivative under control law (14) becomes

$$\begin{aligned}\dot{V}_3 &= -k_1{\xi_1}^2 - k_2{\xi_2}^2 - k_3{\xi_3}^2 \le 0\\ &= -k_1{\xi_1}^2 - k_2{\xi_2}^2 + \xi_3[-(k_1 + k_3 + k_1k_2k_3)z_1\\ &\quad - (k_1k_3 + k_2k_3 + 1)z_2 - k_3z_3 + k_3\ddot{\delta}_{ref}(t)\\ &\quad + (z_2 + k_1z_1)]\\ &= -k_1{\xi_1}^2 - k_2{\xi_2}^2 + \xi_3[-(k_3 + k_1k_2k_3)z_1\\ &\quad - (k_1k_3 + k_2k_3)z_2 - k_3z_3 + k_3\ddot{\delta}_{ref}(t)]\\ &= -k_1{\xi_1}^2 - k_2{\xi_2}^2 + k_3\xi_3[-(1 + k_1k_2)z_1\\ &\quad - (k_1 + k_2)z_2 - z_3 + \ddot{\delta}_{ref}(t)]\end{aligned}$$

Since

$$\begin{aligned}\xi_3 &= z_3 - \alpha_2(\xi_1, \xi_2)\\ &= z_3 - [k_1^2\xi_1 - \xi_1 - k_1\xi_2 - k_2\xi_2 + \ddot{\delta}_{ref}(t)]\\ &= z_3 - [-(1 + k_1k_2)z_1 - (k_1 + k_2)z_2 + \ddot{\delta}_{ref}(t)]\\ &= (1 + k_1k_2)z_1 + (k_1 + k_2)z_2 + z_3 - \ddot{\delta}_{ref}(t)\end{aligned}$$

substitute it to $\dot{V}_3$, there is

$$\dot{V}_3 = -k_1{\xi_1}^2 - k_2{\xi_2}^2 - k_3{\xi_3}^2 \le 0$$

Clearly, based on the supremum and infimum principle, V_3 is bounded when $t\to\infty$. Therefore, ξ_1, ξ_2, ξ_3 are globally bounded. Furthermore, according to the relationship between ξ_1, ξ_2, ξ_3 and z_1, z_2 and z_3, we can draw a conclusion that z_1, z_2 and z_3 are globally bounded.

(II) To prove the asymptotical convergence global of gap $\delta(t)$ and velocity $\dot{\delta}(t)$, we just need to prove $z_1 \to 0$, and $z_2 \to 0$, when $t \to \infty$.

For $\{\xi_1, \xi_2, \xi_3\}$-system, if the Lyapunov function is selected as:

$$V_3 = \frac{1}{2}{\xi_1}^2 + \frac{1}{2}{\xi_2}^2 + \frac{1}{2}{\xi_3}^2$$

$$\dot{V}_3 = -k_1{\xi_1}^2 - k_2{\xi_2}^2 - k_3{\xi_3}^2 \leq 0$$

Obviously, according to the Barbalat's Lemma, there are $\xi_1 \to 0$ and $\xi_2 \to 0$ when $t \to \infty$. As $\xi_1 = z_1$ and $\xi_2 = z_2 + k_1 z_1$, we can obtain $z_1 \to 0$, and $z_2 \to 0$ when $t \to \infty$. Thus, $x_1 \to \delta_{ref}$ and $x_2 \to \dot{\delta}_{ref}$ when $t \to \infty$.

3.3. Switching rule design

While Theorem 1 confirms the stability of the subsystems, it falls short of ensuring the stability of the entire switched system. Therefore, the average dwell time technique is employed to formulate the switching strategy, which is given in Theorem 2.

Theorem 2: For the switched system (6), if it satisfies equations (16) and (17),

$$k_{1,i}\|x\|^2 \leq V(i,t) \leq k_{2,i}\|x\|^2 \tag{16}$$

$$\|x(t)\| \leq \gamma e^{-\varepsilon t}\|x(t_0)\| \tag{17}$$

where $x(t_0)$ is the initial state of the system, and $k_{1,i} \geq 0$, $k_{2,i} \geq 0$, $i = \{1,2\}$, and $\gamma \geq 1$, $\varepsilon > 0$, then the switched system is exponential stable.

Proof: According to the description of the subsection 3.2, the Lyapunov function of the DSS is as follows:

$$V(1,t) = \frac{1}{2}{\xi_1}^2 + \frac{1}{2}{\xi_2}^2 + \frac{1}{2}{\xi_3}^2$$

and the Lyapunov function of the YSS is the same with the DSS's, which can be described as:

$$V(2,t) = \frac{1}{2}{\xi_1}^2 + \frac{1}{2}{\xi_2}^2 + \frac{1}{2}{\xi_3}^2$$

Then, it can be induced as:

$$V(i,t) = \frac{1}{2}{\xi_1}^2 + \frac{1}{2}{\xi_2}^2 + \frac{1}{2}{\xi_3}^2$$

Similar to the derivation of equation (15), there is

$$\dot{V}(i,t) = -k_1{\xi_1}^2 - k_2{\xi_2}^2 - k_3{\xi_3}^2$$

Then,

$$\dot{V}(i,t) \leq -\lambda V(i,t)$$

where the constant $\lambda = \min\{k_i\}(\mathrm{i} = 1,2,3)$, and $\lambda \geq 0$.

According to the comparison lemma, the following equation can be obtained

$$V(i,t) \leq e^{-\lambda(t-t_0)}V(i,t_0)$$

Assuming that the switching time is t_k, $k\in\{1,2,\ldots, N_\sigma\}$, N_σ denotes the switching times of the switching signal during the system's running time. For $N_\sigma > 0$, $N_0 > 0$, if the following equation is satisfied:

$$N_\sigma \leq N_0 + \frac{t-t_0}{T_\sigma}$$

then T_σ is defined as the average dwell time of the switched system. Usually, there is $N_0 = 0$.

If the system switches from subsystem DSS of i to subsystem YSS of j, there is $\sigma_{(t_k^-)} = j$, and $\sigma_{(t_k^+)} = i$.

Given the following equation

$$V(i,t_k) \leq \mu V(j,t_k) \tag{18}$$

By applying an iterative algorithm to equation (18), one obtains

$$\begin{aligned} V(i,t) &\leq e^{-\lambda(t-t_0)}V(i,t_0) \\ &\leq e^{-\lambda(t-t_{k-1})}\mu^2 V(\sigma(t_{k-1}),t_{k-1}^-) \\ &\vdots \\ &\leq e^{-\lambda(t-t_0)}\mu^{N_{\sigma(t,t_0)}}V(\sigma(t_0),t_0) \\ &\leq e^{-\lambda(t-t_0)}\mu^{\frac{t-t_0}{T_\sigma}}V(\sigma(t_0),t_0) \end{aligned} \tag{19}$$

Since

$$\mu^{\frac{t-t_0}{T_\sigma}} = e^{\ln\mu^{\frac{t-t_0}{T_\sigma}}} = e^{\frac{t-t_0}{T_\sigma}\ln\mu} \tag{20}$$

Equation (20) can be further rewritten as:

$$\begin{aligned} V(i,t) &\leq e^{-\lambda(t-t_0)}e^{\frac{t-t_0}{T_\sigma}\ln\mu}V(\sigma(t_0),t_0) \\ &\leq e^{-(t-t_0)(\lambda-\frac{\ln\mu}{T_\sigma})}V(\sigma(t_0),t_0) \end{aligned} \tag{21}$$

According to the DSS and YSS, one can choose $k_{1,1} = k_{1,2} = k_a$, $k_{2,1} = k_{2,2} = k_b$, and by combing with equation (16), the following can be obtained

$$V(2,t) \leq k_b\|x\|^2 \leq \frac{k_b}{k_a}V(1,t)$$

$$V(\sigma(t_0),t_0) \leq k_b\|x(t_0)\|^2$$

Then, according to equation (21), one can obtain

$$\|x(t)\| \leq \left[\frac{V(i,t)}{k_a}\right]^{\frac{1}{2}} \leq \left[\frac{k_b}{k_a}e^{-(\lambda-\frac{\ln\mu}{T_\sigma})(t-t_0)}\right]^{\frac{1}{2}}\|x(t_0)\|$$

where $\gamma = (k_b/k_a)^{1/2}$, $\varepsilon = \lambda/2 - \ln\mu/(2T_\sigma)$, and combining equation (18), there is $\mu = k_b/k_a$. Therefore, the system is exponential stability condition under the proposed switching rule.

4. Case study

According to the established models of DSS and YSS in Section 2, the performance of the proposed method is validated through simulations in Matlab/Simulink environment. The parameters used in the simulation are summarized in Table 1.

Table 1. Parameters of the MYS.

Parameter	Value	Parameter	Value
g	9.8 m/s^2	N	6400
m	500 kg	S	235050 mm^2
R	4.4 Ω	μ_0	$4\pi \times 10^{-7}$ H/m
i_a	$10\sin(\omega t)$ A	ω	1.68 rpm
i_b	$10\sin(\omega t - 120°)$ A	L_q	25 mH
i_c	$10\sin(\omega t + 120°)$ A		

In practical operation conditions, the YSS will operate when the DSS runs to its stable state. In this study, it is assumed that the wind direction changes from 0 s. The variation of the magnetic linkage under the process of the YSS is shown in Figure 4.

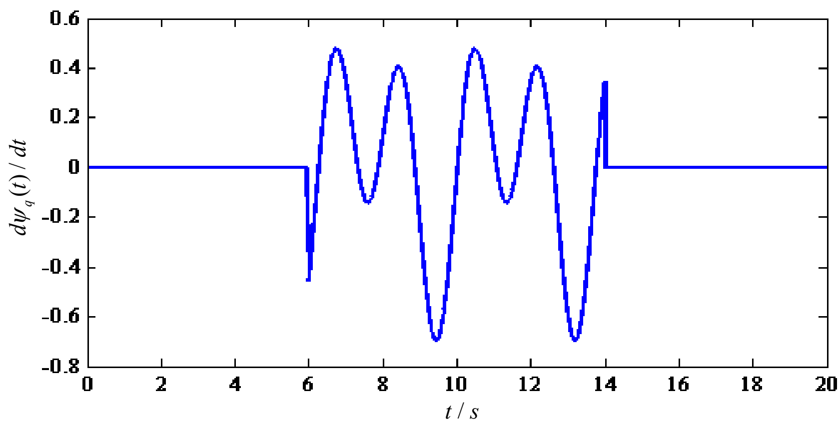

Figure 4. The variation of the magnetic linkage.

The variation of the magnetic linkage would influence the YSS. The proposed controller designed by backstepping method can ensure the stability of YSS. Even though the controller can ensure the stability of the subsystems, if the DSS and YSS switch at any moment without designing the switching rule, it may lead to the instability of the switched system.

The reference trajectories for the DSS and YSS are selected as $0.005e^{-t} + 0.01$ and 0.01 respectively. Then, the state trajectories of DSS and YSS after normalization are shown in Figure 5 and Figure 6, respectively.

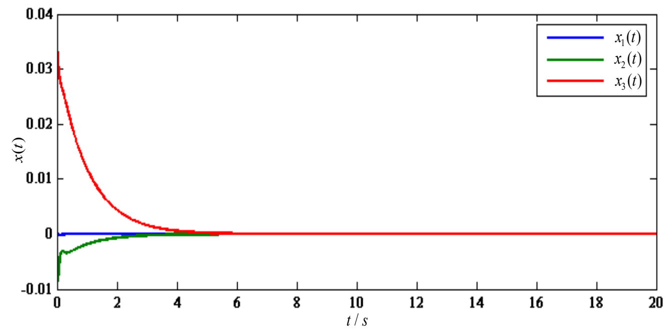

Figure 5. The state trajectory of the DSS.

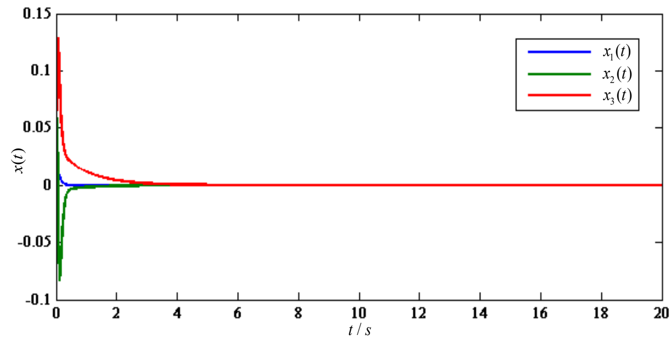

Figure 6. The state trajectory of the YSS.

As demonstrated in Figure 5 and Figure 6, the states x_1, x_2, and x_3 are all stabilize within 6 s, and the states in the YSS even reach stability within 4 s. Thus, the stability of both subsystems is secured through the controllers in Subsection 3.2, affirming the effectiveness of the proposed control scheme. However, the stability of the subsystems cannot ensure the stability of the switched system. Therefore, we need to verify the switched system's stability by average dwell time technique proposed in subsection 3.2.

It is known that if equations (16) and (17) are satisfied, and $\gamma \geq 1$, $\varepsilon > 0$, the switched system satisfies exponentially stability. Due to $\gamma = (k_b/k_a)^{1/2}$, $\varepsilon = \lambda/2 – \ln\mu/(2T_\sigma)$, one chooses $k_a = 1/2$， $k_b = 1$, then, $\mu = 2$, $T_\sigma > \ln\mu/\lambda$. If the parameters are chosen as $k_1 = 30$, $k_2 = 20$, $k_3 = 20$, $\lambda = 2$, then $T_\sigma > 0.35$ s. And we can know that if the average dwell time satisfies $T_\sigma > 0.35$ s, the MYS can guarantee the stable operation not only in each subsystem, but also in the switching system.

In the simulation, the DSS's dwell time is chosen as 6 s, and the YSS's dwell time is 8 s. Figure 7 shows the state trajectory tracking of the system under the average dwell-time switching method.

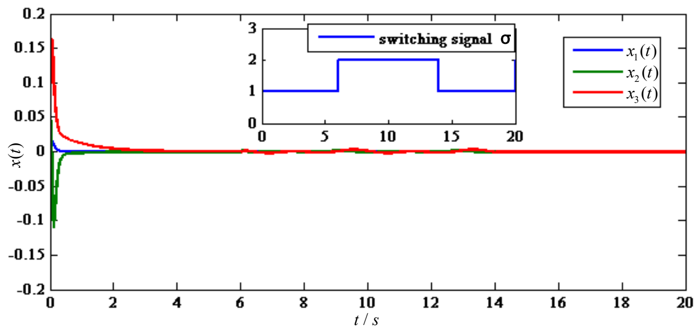

Figure 7. The state trajectory tracking using the average dwell-time switching method.

According to the actual condition, MYS needs to switch into the YSS when the DSS runs to stable state. The running time of YSS needs to be dynamically adjusted according to the variation of wind direction. In this paper, 8 s is assumed to make the YSS run to the wind direction accurately, and then, the system would switch to the DSS. As shown in Figure 7, DSS runs in 0–6 s and 14–20 s respectively, and YSS works in 6–14 s.

As shown in Figure 7, the MYS runs in the process of DSS at first (0 s–6 s), then, it switches to the process of YSS until the DSS is stable. Subsequently, the YSS runs 8s (6 s–14 s) to make the MYS yaw to the wind direction. After that, it switches to the DSS again (14 s–20 s). Despite the mode changes occurring around $t = 5$ s, $t = 10$ s, and $t = 15$ s, the system states x_1, x_2, and x_3 remain uniformly bounded and converge smoothly to the equilibrium. The results confirm that the proposed switching controller is effective and that the system remains stable under the average dwell time approach.

To further assess the proposed switching rule's effectiveness, a comparative experiment is conducted using a dwell-time (fixed-time) switching system. In the simulation, the dwell time of both DSS and YSS is set to 10 s, while the system switches every 5 s in a fixed manner. Figure 8 shows the state trajectory tracking of the system under the dwell-time switching method.

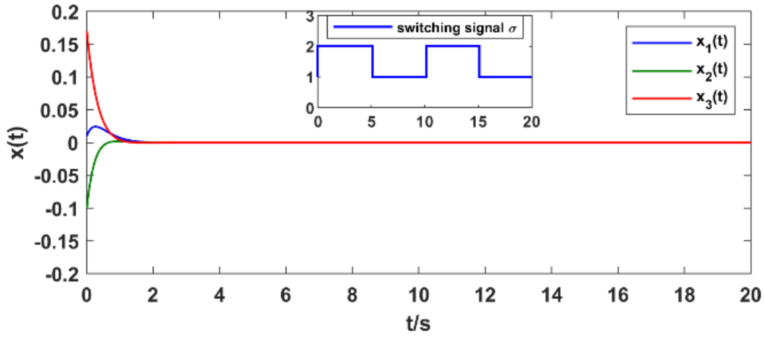

Figure 8. The state trajectory tracking of the system under the dwell-time switching method.

From Figure 8, it can be observed that the convergence of state x_3 is faster compared to that in Figure 7. However, the convergence speeds of states x_1 and x_2 are noticeably slower than those under the ADT method shown in Figure 7. Moreover, the switching rule in Figure 7 is more flexible, enabling more adaptive transitions between subsystems. In contrast, the system in Figure 8 follows a strict fixed dwell-time rule, requiring a minimum dwell time to be satisfied before each switch occurs. In summary, the ADT method offers clear advantages over the dwell-time switching approach.

5. Conclusions

In this study, precise mathematical models of the DSS and YSS have been established. Since the stability of each subsystem is required in the MYS, the stable controllers of the DSS and YSS are designed by backstepping approach. However, the stability of single subsystem cannot ensure the stability of switched system. Therefore, in order to ensure the switching stability between DSS and YSS, the average dwell time is applied to design the switching rule to ensure the stability of the switched system. Finally, the simulation results show that the proposed method can guarantee the stability not only in each subsystem process, but also in the whole switched system.

Future research will concentrate on enhancing the trajectory tracking process, developing a mathematical model of the MYS in yawing mode, and designing stable switching strategies among the three operational modes: levitation, yawing, and landing. In addition, the proposed switching controller will be further extended by incorporating yaw misalignment effects and evaluating its combined impact on energy efficiency, even under faults, disturbances, and varying load conditions.

Acknowledgements

This work is supported by the National Natural Science Foundation of China under Grant 62303414, China Postdoctoral Science Foundation under Grant 2023M741821, Natural Science Foundation of Zhejiang Province under Grant LQ23F030016, Zhejiang Province Postdoctoral Selected Foundation under Grant No. ZJ2023143.

Authors' contribution

Conceptualization, Xiuli Wang and Jianye Gong; methodology, Xiuli Wang; software, Qingyang Chen; validation, Xiuli Wang, Qingyang Chen and Jianye Gong; formal analysis, Xiuli Wang; investigation, Xiuli Wang; resources, Qingyang Chen; data curation, Qingyang Chen; writing—original draft preparation, Xiuli Wang and Qingyang Chen; writing—review and editing, Jianye Gong; visualization, Qingyang Chen; supervision, Jianye Gong; project administration, Xiuli Wang; funding acquisition, Xiuli Wang. All authors have read and agreed to the published version of the manuscript.

Conflicts of interests

The authors declare no conflict of interest.

References

[1] Li Y, Cai B, Song X, Chu X, Su B. Modeling of maglev yaw system of wind turbines and its robust trajectory tracking control in the levitating and landing process based on NDOB. *Asian J. Control* 2019, 21(2):770–782.

[2] Magnus DM, Scharlau CC, Pfitscher LL, Costa GC, Silva GM. A novel approach for robust control design of hidden synthetic inertia for variable speed wind turbines. *Electr. Power Syst. Res.* 2021, 196:107267.

[3] Xu F, Lu X, Zheng T, Xu X. Motion control of a magnetic levitation actuator based on a wrench model considering yaw angle. *IEEE Trans. Ind. Electron.* 2019, 67(10):8545–8554.

[4] El Asri B. Optimal multi-modes switching problem in infinite horizon. *Stochastics Dyn.* 2010, 10(2):231–261.

[5] Suzuki K. Infinite-horizon optimal switching regions for a pair-trading strategy with quadratic risk aversion considering simultaneous multiple switchings: a viscosity solution approach. *Math. Oper. Res.* 2021, 46(1):336–360.

[6] Su Q, Fan Z, Lu T, Long Y, Li J. Fault detection for switched systems with all modes unstable based on interval observer. *Inf. Sci.* 2020, 517:167–182.

[7] Liberzon D. *Switching in systems and control*, 1st ed. Boston: Birkhauser, 2003.

[8] Wang Y, Hu X, Shi K, Song X, Shen H. Network-based passive estimation for switched complex dynamical networks under persistent dwell-time with limited signals. *J. Franklin Inst.* 2020, 357(15):10921–10936.
[9] Yang X, Liu Y, Cao J, Rutkowski L. Synchronization of coupled time-delay neural networks with mode-dependent average dwell time switching. *IEEE Trans. Neural Networks Learn. Syst.* 2020, 31(12):5483–5496.
[10] Ma L, Xu N, Huo X, Zhao X. Adaptive finite-time output-feedback control design for switched pure-feedback nonlinear systems with average dwell time. *Nonlinear Anal. Hybrid Syst*. 2020, 37:100908.
[11] Ma R, An S, Fu J. Dwell-time-based stabilization of switched positive systems with only unstable subsystems. *Sci. China Inf. Sci.* 2021, 64(1):119205.
[12] Zhang P, Kao Y, Hu J, Niu B, Xia H, *et al*. Finite-time observer-based sliding-mode control for Markovian jump systems with switching chain: average dwell-time method. IEEE *Trans. Cybern.* 2021, 53(1):248–261.
[13] Zeng D, Liu Z, Chen CLP, Wang Y, Zhang Y, *et al*. Adaptive neural prescribed-time control of switched nonlinear systems with mode-dependent average dwell time. *IEEE Trans. Syst. Man Cybern.: Syst.* 2023, 53(12):7427–7440.
[14] Nojoumian MA, Zakerzadeh MR, Ayati M. Stabilization of delayed switched positive nonlinear systems under mode dependent average dwell time: a bumpless control scheme. *Nonlinear Anal. Hybrid Syst.* 2023, 47:101300.
[15] Philippe M, Essick R, Dullerud GE, Jungers RM. Stability of discrete-time switching systems with constrained switching sequences. *Automatica* 2016, 72:242–250.
[16] Dercole F, Della Rossa F. Tree-based algorithms for the stability of discrete-time switched linear systems under arbitrary and constrained switching. *IEEE Trans. Autom. Control* 2018, 64(9):3823–3830.
[17] Li X, Liu K, Liu H, Wang Y. New input-to-state stability results on switched delay systems under arbitrary switching. *Int. J. Control* 2023, 96(3):593–598.
[18] Della Rossa M, Egidio LN, Jungers RM. Stability of switched affine systems: arbitrary and dwell-time switching. *SIAM J. Control Optim.* 2023, 61(4):2165–2192.
[19] Ding X, Lu J, Li H. Stability of logical dynamic systems with a class of constrained switching. *IEEE Trans. Circuits Syst. I Regul. Pap.* 2022, 69(10):4248–4257.
[20] Ren W, Xiong J. Stochastic stability of impulsive switched systems with constrained switching and impulses. *IEEE Control Syst. Lett.* 2020, 5(4):1441–1446.